

# THE STRATOSPHERE–TROPOSPHERE ANALYSES OF REGIONAL TRANSPORT 2008 EXPERIMENT

BY LAURA L. PAN, KENNETH P. BOWMAN, ELLIOT L. ATLAS, STEVE C. WOFSY, FUQING ZHANG, JAMES F. BRESCH,  
BRIAN A. RIDLEY, JASNA V. PITTMAN, CAMERON R. HOMEYER, PAVEL ROMASHKIN, AND WILLIAM A. COOPER

START08 combined high-altitude long-range aircraft, new chemical instrumentation, and high-resolution meteorological models to map the chemical and microphysical structure and the major transport processes in the extratropical upper troposphere and lower stratosphere.

**NSF/NCAR Gulfstream V (GV) aircraft at Rocky Mountain Metro Airport, Broomfield, Colorado, ready for the first START08 research flight, on April 18, 2008. (Photo: James Bresch)**

**BACKGROUND AND MOTIVATIONS.** During the arms race after World War II, several nations conducted atmospheric tests of nuclear weapons. It was thought these tests would be safe, in that most radioactive particles would fall out close to the test site while the remainder would decay harmlessly in the stratosphere before eventually falling into the troposphere. However, radioactivity appeared in eastern North American food only days after weapons tests. In response, ground-breaking meteorological studies were carried out that discovered processes responsible for rapid exchange of air between the stratosphere and troposphere (e.g., Reed 1955; Danielsen 1968). Over the next half century, ►

the study of stratosphere–troposphere exchange (STE) brought new understanding to many aspects of atmospheric science beyond that of radioactive fallout. The upper troposphere (UT) and lower stratosphere (LS) are now known to be strongly coupled through transport processes that are driven by both weather systems and large-scale stratosphere circulations (Holton et al. 1995).

Chemically, the UT and LS have distinct air masses. The stratosphere is rich in ozone but extremely dry, with ~5 ppmv of water vapor. The troposphere is relatively ozone poor but moist. The chemical gradients across the tropopause, especially those of water vapor and ozone, are important components of Earth’s radiative balance (e.g., Forster and Shine 1997; Shepherd 2007). Because many trace constituents have relatively long lifetimes in this part of the atmosphere, transport processes play a critical role in determining trace species distributions. Many meteorological phenomena such as Rossby waves, gravity waves (GWs), jets

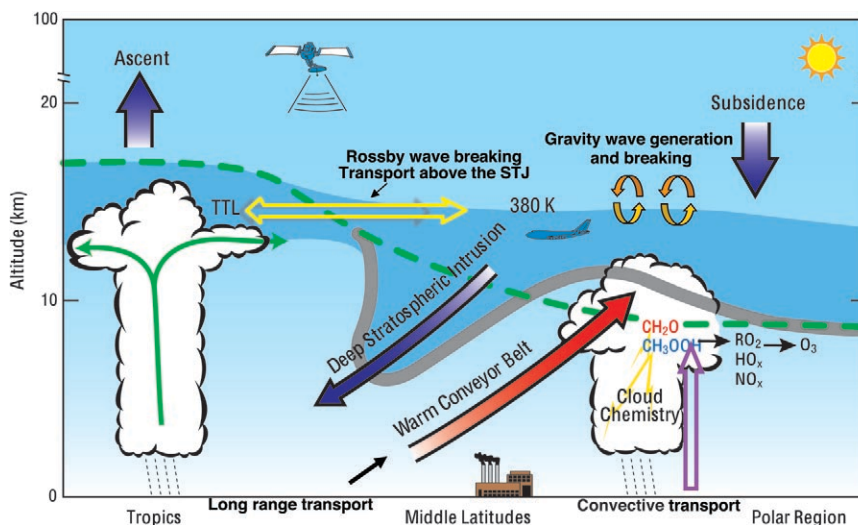


**FIG. 1.** This schematic (based on Stohl et al. 2003) portrays important processes that couple dynamics, chemistry, and cloud microphysics in the UTLS region. START08 targeted major transport processes that are indicated by bold arrows. The dashed green line represents the time-averaged tropopause. In the tropics, maximum outflow from deep convection occurs near ~12–14 km, while the cold-point tropopause occurs near 17 km. The intervening region has characteristics intermediate between the troposphere and stratosphere and is termed the tropical transition layer (TTL). Extratropical STE occurs in tropopause folds and intrusions linked with synoptic weather systems; these events transport stratospheric air high in ozone into the troposphere. Transport above the subtropical jet (STJ) couples the TTL and the extratropical LS. In addition, synoptic-scale uplift (“warm conveyor belts”) and deep convection brings near-surface emissions of gases and particles into the upper troposphere, where they can strongly influence global-scale chemistry. Here GW generation and breaking also contribute to the mixing of chemical constituents in the UTLS.

and upper-level fronts, baroclinic disturbances, and convection have ramifications for chemical transport. UTLS transport, therefore, is an important link in chemistry–climate interactions. For example, will changing weather patterns in a future climate redistribute radiatively significant chemical species and pollutants? For these reasons, evaluating and improving the representation of UTLS transport in global Chemistry–Climate Models (CCMs) is a key element of the ongoing CCM validation (CCMVal) activity (Eyring et al. 2005).

Significant progress on these problems has been made in the last 10 years using newly available high-resolution meteorological analyses and Lagrangian models (Stohl et al. 2003; Sprenger and Wernli 2003; Wernli and Sprenger 2007). These analyses provided a global perspective of preferred locations of STE based on the variability of the meteorological fields. In parallel with model studies, aircraft observations have shown that relationships among chemical constituents can be used to diagnose STE and mixing

**AFFILIATIONS:** PAN, BRESCH, RIDLEY, PITTMAN, ROMASHKIN, AND COOPER—National Center for Atmospheric Research, Boulder, Colorado; BOWMAN, ZHANG, AND HOMEYER—Texas A&M University, College Station, Texas; ATLAS—University of Miami, Miami, Florida; WOFSY—Harvard University, Cambridge, Massachusetts; ZHANG—Pennsylvania State University, University Park, Pennsylvania

**CORRESPONDING AUTHOR:** Laura L. Pan, National Center for Atmospheric Research, P.O. Box 3000, Boulder, CO 80307–3000  
E-mail: liwen@ucar.edu

The abstract for this article can be found in this issue, following the table of contents.

DOI:10.1175/2009BAMS2865.1

In final form 14 September 2009  
©2010 American Meteorological Society

across the tropopause (e.g., Hintsala et al. 1998; Zahn et al. 2000; Fischer et al. 2000; Hoor et al. 2002, 2004; Pan et al. 2004; Marcy et al. 2004; Pan et al. 2007). Despite significant progress, quantifying STE remains a challenge. A detailed understanding of the connections between dynamical processes and tracer distributions is yet to be established.

Motivated by the needs for process studies and diagnosis of CCMs, the Stratosphere–Troposphere Analyses of Regional Transport 2008 (START08) experiment was conducted, using the new National Science Foundation (NSF)–National Center for Atmospheric Research (NCAR) Gulfstream V (GV) research aircraft, also known as the High-Performance Instrumented Airborne Platform for Environmental Research (HIAPER). The experiment was designed to establish a better connection between the chemical structure of the UTLS region and atmospheric dynamics. A primary hypothesis was that measurements of chemical distributions in well-defined meteorological conditions could be used to identify tracer signatures associated with the key transport processes near the extratropical tropopause. The investigation focused on the behavior of the extratropical tropopause as a transport boundary and on the chemical distributions and relationships associated with dynamical processes in the UTLS (see Fig. 1). The contributing dynamical processes include the breaking of Rossby waves; the growth and decay of synoptic-scale waves, tropopause folds, and warm conveyor belts; the development of frontal systems; the initiation and breaking of gravity waves; and deep convection.

START08 built upon the results and experience of the START05 experiment during the initial flights of the GV aircraft. In addition to demonstrating the utility of the GV for UTLS studies, START05 flights observed aerosol formation (Young et al. 2007), large-scale transport (Bowman et al. 2007), and the chemical structure of the tropopause (Pan et al. 2007). The operational capabilities of the GV aircraft developed during START05 were essential for planning the more complex payload and goals of START08.

START08 was conducted during April–June 2008. A comprehensive suite of trace gas and microphysical measurements was made in the tropopause region using the GV, operating from the NCAR aviation facility in Broomfield, Colorado. START08 shared its payload and flight operations with test flights of the HIAPER Pole-

to-Pole Observation of Atmospheric Tracers (pre-HIPPO) experiment. Eighteen research flights (RFs) totaling 123 flight hours were flown during 6 weeks of operations: flights 1–12 during the spring phase (15 April–16 May) and flights 13–18 during the summer phase (12–28 June). Extensive coverage of central North America (25°–65°N, 80°–120°W; Fig. 2) and altitudes from the surface to ~14.3 km were achieved. The measurements targeted a number of different meteorological scenarios, including intrusions of stratospheric air into the troposphere by tropopause folding, intrusions of tropospheric air into the lower stratosphere associated with double tropopause events, gravity wave generation by jets and fronts, and convective transport to the upper troposphere. Several flights surveyed the extratropical troposphere and stratosphere, with many tropopause crossings. The observations of chemical tracer variation and tracer–tracer correlations will provide a set of “fingerprints” that relate the meteorological fields and the UTLS chemical distributions.

This overview describes the observational aspects of the experiment, provides background information for the research community, and gives some highlights based on preliminary analyses. The initial results indicate many possible areas of impact and the broad reach of the experiment. Data analyses are ongoing by the science team and current collaborators. We invite the interest of the broader community

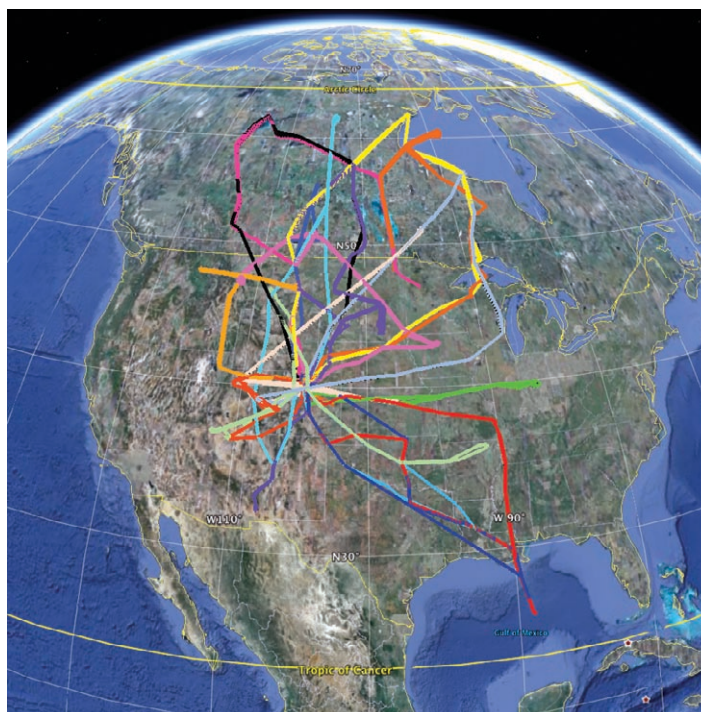


**Fig. 2.** GV ground tracks for the 18 research flights.

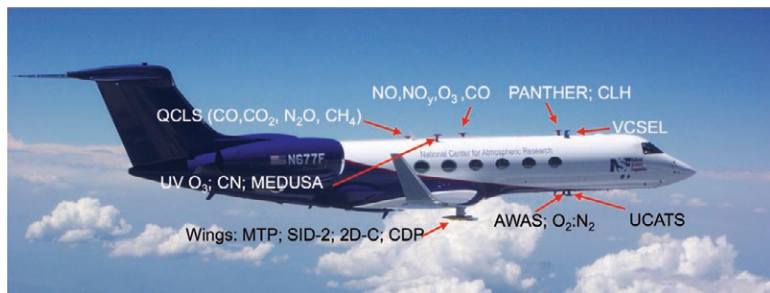


**FIG. 3. GV in flight as viewed during an airborne comparison during START08. Inlet locations for the 18 research instruments are marked.**

to utilize the START08 data for their research. The aircraft data are archived at the National Center for Atmospheric Research for public use and are available online (at [www.eol.ucar.edu/projects/start08/START08\\_HomePage.html](http://www.eol.ucar.edu/projects/start08/START08_HomePage.html)).

**DESIGN OF THE EXPERIMENT.** *Platform and payload.* The GV research aircraft is ideally suited for

investigating the extratropical tropopause region. With the START08 payload its ceiling is ~14.3 km, which is well above the typical extratropical tropopause, allowing measurements in the lower stratosphere. Its flight duration of ~8 h enables the GV to sample a large geographic area in a single flight. A GV flight can include multiple profiles from the boundary layer to the lower stratosphere. With these capabilities, the GV can provide high-resolution *in situ* observations

of synoptic-scale chemical and dynamical structures as well as long-range surveys. At cruise altitude, each sample in 1-Hz observations typically represents an air mass of 200–250 m in horizontal scale.

In addition to standard measurements of atmospheric state variables, the GV carried 18 research instruments that measured a large suite of chemical species and microphysical parameters (Fig. 3;

**TABLE 1. GV research instrument payload. HAIS = HIAPER Aircraft Instrument Solicitation.**

Instrument	Measurement	Name of principal investigator, Institute
<b>Chemical tracers</b>		
AWAS	See Table 2	Atlas, HAIS/University Miami
Quantum cascade laser system (QCLS)	CO <sub>2</sub> , CO, CH <sub>4</sub> , N <sub>2</sub> O	Wofsy, HAIS/Harvard University
Fast ozone (Fast-O3)	O <sub>3</sub>	Weinheimer, HAIS/NCAR
Total reactive odd-nitrogen and nitric oxide	NO <sub>y</sub> , NO	Weinheimer, NCAR
Dual-beam UV absorption ozone photometer	O <sub>3</sub>	Gao, NOAA/ESRL/CSD
VUV resonance fluorescence	CO	Campos, NCAR
Open path tunable diode laser hygrometer	H <sub>2</sub> O vapor	Campos, NCAR
Vertical cavity surface emitting laser hygrometer (VCSEL)	H <sub>2</sub> O vapor	Zondlo, HAIS/SWS
UAS UCATS	H <sub>2</sub> O, O <sub>3</sub> , N <sub>2</sub> O, SF <sub>6</sub> , H <sub>2</sub> , CH <sub>4</sub> , CO	Hurst/Elkins, NOAA/University of Colorado
PANTHER	See Table 2.	Moore/Elkins, NOAA
Airborne oxygen instrument (AO2)	O <sub>2</sub> :N <sub>2</sub>	Stephens, NCAR/RAF
Multiple enclosure device for unfractionated sampling of air (MEDUSA)	O <sub>2</sub> :N <sub>2</sub> , Ar:N <sub>2</sub> , <sup>13</sup> CO <sub>2</sub> , C <sup>18</sup> OO	Stephens, NCAR/RAF
<b>Cloud microphysics</b>		
Closed-path tunable diode laser hygrometer (CLH)	Total water	Avallone, University of Colorado
Small ice detector-2H (SID2)	Small ice (2–60 mm)	Heymsfield, HAIS/NCAR
2-D cloud particle imaging probe (2DC)	Ice + rain (25–1600 mm)	Cooper, NCAR/RAF
Cloud droplet probe (CDP)	Cloud drop (2–60 mm)	Cooper, NCAR/RAF
Condensation nuclei (water-CN)	Condensation nuclei	Rogers, NCAR/RAF
<b>Remote sensing</b>		
Microwave temperature profiler (MTP)	Temperature profile	Mahoney, HAIS/JPL

Table 1). Among the chemical species, ozone, water vapor, and carbon monoxide are the most important and widely used for diagnosis of transport. Carbon dioxide, methane, and nitrous oxide are long-lived tracers for transport and for identifying anthropogenic and biogenic influences. Nitric oxide and total reactive nitrogen (NO/NO<sub>y</sub>), in addition to transport, provide information about the impact of pollution,

aircraft emissions, and lightning sources to the UTLS. Sulfur hexafluoride and carbon dioxide have been widely used to diagnose the age of air in the stratosphere through comparisons with well-defined temporal trends in the troposphere. A large suite of constituents with a variety of chemical lifetimes was measured by the Advanced Whole Air Sampler (AWAS), the Peroxyacetyl Nitrate (PAN) and other

**TABLE 2. Trace gas measurements from the HAIS AWAS and PANTHER/UCATS instruments.**

	PAN- THER/ UCATS	AWAS		PAN- THER/ UCATS	AWAS
<b>Chlorofluorocarbons</b>			<b>Organic nitrates</b>		
CFC-11 (CCl <sub>3</sub> F)	✓	✓	Methyl nitrate(CH <sub>3</sub> ONO <sub>2</sub> )		✓
CFC-12 (CCl <sub>2</sub> F <sub>2</sub> )	✓	✓	Ethyl nitrate(C <sub>2</sub> H <sub>5</sub> ONO <sub>2</sub> )		✓
CFC-113 (CCl <sub>2</sub> FCClF <sub>2</sub> )		✓	Propyl nitrates(C <sub>3</sub> H <sub>7</sub> ONO <sub>2</sub> )		✓
CFC-114 (CClF <sub>2</sub> CClF <sub>2</sub> )		✓	Butyl nitrates (C <sub>4</sub> H <sub>9</sub> ONO <sub>2</sub> )		✓
<b>Halons</b>			Pentyl nitrates (C <sub>5</sub> H <sub>11</sub> ONO <sub>2</sub> )		✓
CFC-12b1 (Halon 1211,CF <sub>2</sub> ClBr)	✓	✓	Peroxyacetyl nitrate (CH <sub>3</sub> C(O)OONO <sub>2</sub> )	✓	
CFC-13b1 (Halon 1301, CF <sub>3</sub> Br)		✓	<b>Nonmethane hydrocarbons</b>		
CFC-114b2 (Halon 2402, C <sub>2</sub> F <sub>4</sub> Br <sub>2</sub> )		✓	Ethane (C <sub>2</sub> H <sub>6</sub> )		✓
<b>Hydrochlorofluorocarbons/hydrofluorocarbons</b>			Ethyne (C <sub>2</sub> H <sub>2</sub> )		✓
HCFC-22 (CHF <sub>2</sub> Cl)	✓	✓	Propane(C <sub>3</sub> H <sub>8</sub> )		✓
HCFC-141b (CH <sub>3</sub> CFCl <sub>2</sub> )	✓	✓	Isobutane(C <sub>4</sub> H <sub>10</sub> )		✓
HCFC-142b (CH <sub>3</sub> CF <sub>2</sub> Cl)	✓	✓	n-Butane (C <sub>4</sub> H <sub>10</sub> )		✓
HFC-134a (C <sub>2</sub> H <sub>2</sub> F <sub>4</sub> )	✓	✓	Isopentane (C <sub>5</sub> H <sub>12</sub> )		✓
HCFC-124 (C <sub>2</sub> HClF <sub>4</sub> )		✓	n-Pentane (C <sub>5</sub> H <sub>12</sub> )		✓
HCFC-123 (C <sub>2</sub> HCl <sub>2</sub> F <sub>3</sub> )		✓	Isoprene (C <sub>5</sub> H <sub>10</sub> )		✓
HFC-152a (CH <sub>3</sub> CHF <sub>2</sub> )		✓	Benzene (C <sub>6</sub> H <sub>6</sub> )		✓
<b>Solvents</b>			Toluene (C <sub>7</sub> H <sub>8</sub> )		✓
Carbon tetrachloride (CCl <sub>4</sub> )		✓	C <sub>2</sub> -Benzenes (C <sub>8</sub> H <sub>10</sub> )		✓
Methyl chloroform(CH <sub>3</sub> CCl <sub>3</sub> )		✓	<b>Other</b>		
Tetrachloroethylene (C <sub>2</sub> Cl <sub>4</sub> )		✓	Methane (CH <sub>4</sub> )	✓	✓
Methylene chloride (CH <sub>2</sub> Cl <sub>2</sub> )		✓	Carbon monoxide (CO)	✓	✓
Chloroform (CHCl <sub>3</sub> )		✓	Nitrous oxide (N <sub>2</sub> O)	✓	✓
Trichloroethylene(C <sub>2</sub> HCl <sub>3</sub> )		✓	Hydrogen (H <sub>2</sub> )	✓	
1,2-Dichloroethane (C <sub>2</sub> H <sub>4</sub> Cl <sub>2</sub> )		✓	Carbonyl sulfide (COS)	✓	✓
<b>Methyl halides and related compounds</b>			Dimethyl sulfide (C <sub>2</sub> H <sub>6</sub> S)		✓
Methyl bromide(CH <sub>3</sub> Br)	✓	✓	Carbon disulphide (CS <sub>2</sub> )	✓	
Methyl chloride (CH <sub>3</sub> Cl)	✓	✓	Methyl-t-butyl ether (C <sub>5</sub> H <sub>12</sub> O)		✓
Methyl iodide (CH <sub>3</sub> I)	✓	✓	Methyl acetate/ethyl acetate		✓
Methylene bromide(CH <sub>2</sub> Br <sub>2</sub> )		✓	Acetonitrile (CH <sub>3</sub> CN)		✓
CH <sub>x</sub> Br <sub>y</sub> Cl <sub>z</sub>		✓	1,2 Dichlorobenzene (C <sub>6</sub> H <sub>4</sub> Cl <sub>2</sub> )		✓
Bromoform (CHBr <sub>3</sub> )		✓	<b>Perfluorocarbons</b>		
Ethyl bromide (C <sub>2</sub> H <sub>5</sub> Br)		✓	Sulfur hexafluoride (SF <sub>6</sub> )	✓	
n-Propyl bromide (C <sub>3</sub> H <sub>7</sub> Br)		✓			

Trace Hydrohalocarbon Experiment (PANTHER), and Unmanned Aircraft Systems (UAS) Chromatograph for Atmospheric Trace Species (UCATS) instruments (Table 2). These tracers provide complementary information for identifying the origin of air masses and the time scale of processes involved. For the microphysical studies, water vapor, total water, and ice particle measurements over the size range of 2–1600  $\mu\text{m}$  were made.

*Flight scenarios.* The objectives of START08 were addressed by a set of prioritized flight scenarios, each designed for specific objectives. The scenarios are as follows:

- UTLS survey—to obtain constituent distributions and tracer relationships across the tropopause for a range of thermal and dynamical conditions
- Stratospheric intrusions—to investigate stratospheric influence on the troposphere by mixing and irreversible transport during tropopause folds
- Tropospheric intrusions—to study the origins and fate of air with tropospheric characteristics in the lower stratosphere
- Convective influence—to investigate UT tracer distributions influenced by convective transport and lightning and to explore flight strategies for measuring the influence of storms
- Cirrus layers—to examine cirrus cloud layers near the extratropical tropopause
- Gravity waves—to observe the properties of gravity waves generated by multiple sources, including jets/fronts and topography
- Pre-HIPPO—to test instrument and aircraft performance while profiling from the boundary layer to the tropopause, a strategy needed for the global HIPPO project

Each of the 18 flights was planned around one primary objective but often contributed to additional objectives. Examples of several major flight scenarios are discussed in next section.

*Forecasting, nowcasting, and in-flight decision making.* Accurate and reliable forecasts and nowcasts were critical to the success of the START08 experiment. There were several challenging factors. Because the mission objectives relied on specific meteorological conditions, there was a need to identify possible flight options several days in advance. Furthermore, the relatively short time period of the experiment and the need to meet the multiple objectives of the

mission required flights roughly every other day. These factors demanded multiday flight planning. During the campaign, forecasts were made over large geographic regions approximately 18 h in advance of each flight to optimize the range and the duration of the GV flights and to accommodate the relatively long preflight preparations required by the chemical instrumentation.

Forecasting and flight planning were supported with multiple models and tools. The primary model for flight planning was the National Centers for Environmental Prediction's (NCEP) Global Forecast System (GFS) operational model converted from its native-grid resolution of T382L64 to a  $0.325^\circ \times 0.325^\circ$  grid with 47 pressure levels. For this mission we used twice-daily forecasts (0000 and 1200 UTC) out to 54 h. Custom tools for interactively displaying cross sections of the GFS model output were developed by the team to visualize the tropopause structure, jet position, potential vorticity (PV), and intrusions. The GFS ensemble forecasts were used for longer-range logistical planning. In addition, high-resolution Advanced Research Weather Research and Forecasting (WRF; Skamarock et al. 2005) forecasts were produced at Texas A&M (15-km-resolution single run and a 45-km-resolution ensemble initialized with a mesoscale ensemble-based multiphysics data assimilation system; Meng and Zhang 2008a,b) and NCAR (20-km-resolution initialized with GFS analysis) to provide additional guidance.

Nowcasts were provided to the onboard mission scientist to support in-flight decisions. It was an essential element for the success of all flight scenarios, and it was most critical during flights near convective systems. Satellite imagery, radar reflectivity, and information from NCEP's Rapid Update Cycle (RUC) model were combined with real-time observations from the GV to guide in-flight decisions for altitude or course changes. The real-time data display capability on board the GV was a critical component of in-flight decision-making. Chemical tracers such as ozone, CO, and  $\text{H}_2\text{O}$  were among the most valuable indications of airmass type and airmass boundaries. Temperature and wind speed were essential for identifying GV position relative to the jet structure. The GV's position was monitored in realtime by displaying the flight track using Google Earth, which has the capability of overlaying low-resolution satellite or radar imagery. Weather updates were continuously provided to the onboard mission scientists using Internet Relay Chat (IRC), which proved to be an excellent means of communication between the air and ground

**Satellite data and modeling.** The in situ aircraft measurements are complemented by global satellite data analyses and multiscale models. Near-real-time data from the Atmospheric Infrared Sounder (AIRS) on the National Aeronautics and Space Administration (NASA) *Aqua* satellite, the Infrared Atmospheric Sounding Interferometer (IASI) on the European meteorological polar-orbiting satellite *MetOp-A*, and the Microwave Limb Sounder (MLS) on the NASA *Aura* satellite were produced for the experiment to provide a broader context for the GV flights. To connect the observations with the state-of-art models and to quantify observed transport, a set of model studies was planned as a part of the experiment. In particular, the NCAR Whole Atmosphere Community Climate Model (WACCM; Garcia et al. 2006; Kinnison et al. 2007) was used to simulate the meteorology and chemistry of the experiment period. The high-resolution Lagrangian chemical transport model [Chemical Lagrangian Model of the Stratosphere (CLaMS); McKenna et al. 2002; Konopka et al. 2007] will be used in postmission analyses to examine the transport and mixing observed in the experiment. High-resolution cloud-resolving simulations with the Advanced Research WRF model are also part of the postcampaign modeling effort.

**EXPERIMENT HIGHLIGHTS.** All seven of the flight scenarios were successfully accomplished during the experiment. Most of the objectives were investigated on multiple flights. Here we present selected results that highlight some of the major processes examined during START08.

**Tropospheric intrusion: RF01, 18 April 2008.** The existence of multiple tropopauses has been known for more than a half century (e.g., Palmén and Newton 1969; Kochanski 1955). Evidence of subtropical tropospheric air intruding deep into the extratropical lower stratosphere has also been observed as low-ozone laminae in ozonesonde data for several decades (Dobson 1973; Vaughan and Timmis 1998). Only recently has it been unambiguously identified, using satellite data and high-resolution meteorological analyses, that these low-ozone laminae are part of stratified structures associated with the occurrence of the secondary (double) tropopause (Pan et al. 2009). Furthermore, analyses based on extensive coverage by spaceborne GPS measurements indicate that double tropopause events are more common than previously documented (e.g., Schmidt et al. 2006; Randel et al. 2007). Thus, the question is how and to what extent this type of event perturbs the chemical composition of the lower stratosphere. Such events are capable

of bringing tropical air (often of a photochemically young age, containing more reactive species) into the stratospheric overworld (Holton et al. 1995) at high latitudes. The transport mechanism, spatial structure, chemical composition, and impact on the lower stratosphere are among the major issues that START08 was designed to address.

Forecasts of tropospheric intrusions were made using the high-resolution GFS data. Following the method demonstrated in Pan et al. (2009), the GFS temperature forecasts were used to identify regions with a double tropopause. The minimum static stability between the two tropopauses and the altitude of the minimum were calculated and used for flight planning. Figure 4 shows the horizontal extent of the area with a double tropopause, based on GFS, over North America at 1800 UTC 18 April 2008 and the GV ground track for RF01. The minimum static stability between the primary and secondary tropopauses is given by the color shading. The purple and blue shadings indicate regions where this layer has near-tropospheric static stability. This layer is located ~3 km above the primary tropopause (see Fig. 5a) and well north of the tropopause break associated with the subtropical jet, which lies along the southern edge of the United States.

A triangular flight path with several vertical profiles was carried out to sample the vertical and horizontal structures of the air mass associated with the intrusion. Figure 5a shows the first leg of the GV flight track and the vertical section of the along-track static stability ( $d\theta/dz$ ), which went northeastward from Colorado to near the shore of Hudson Bay, Canada. The cross section of the static stability shows a layered structure with two stable layers, one near 300 hPa, associated with the primary tropopause, and one above 100 hPa, associated with a secondary tropopause. The layer of low-stability air in between is centered around 150 hPa (~14 km altitude, 380 K potential temperature). Vertical gradients of trace species were measured for the altitude range from the upper troposphere to the center of the low-stability layer. The primary tracers,  $O_3$  and CO, are consistent with the dynamic variables in GFS analyses, showing a sharp increase of ozone as the GV entered the stratosphere and immediately dropped back to near-tropospheric levels in the low-stability layer. The behavior of the tropospheric tracer, CO, is opposite to that of  $O_3$ , as expected. Together, the data reveal anomalous values of  $O_3$  (~150 ppbv) and CO (~50 ppbv) at 380 K near 50°N.

Although this is the largest tropospheric intrusion event observed during START08, the influence of this type of event was seen many times during the experi-

ment. As a result, anomalous values are observed in all long-lived chemical tracers and many intermediate lifetime tracers. Figure 6 shows the tropopause referenced vertical profiles of selected tracers. The signatures of the tropospheric intrusion are groups of anomalous points ~3 km above the tropopause. These points are separated from the expected stratospheric behavior for the long-lived tracers (months–years; O<sub>3</sub> and N<sub>2</sub>O are given as examples). The signature is no longer as apparent for the shorter-lived species, such as C<sub>4</sub>H<sub>10</sub> (isobutane), which has a lifetime of ~10 days. The impact of these events on the age spectrum of the extratropical lower stratosphere will be a focus of further analysis.

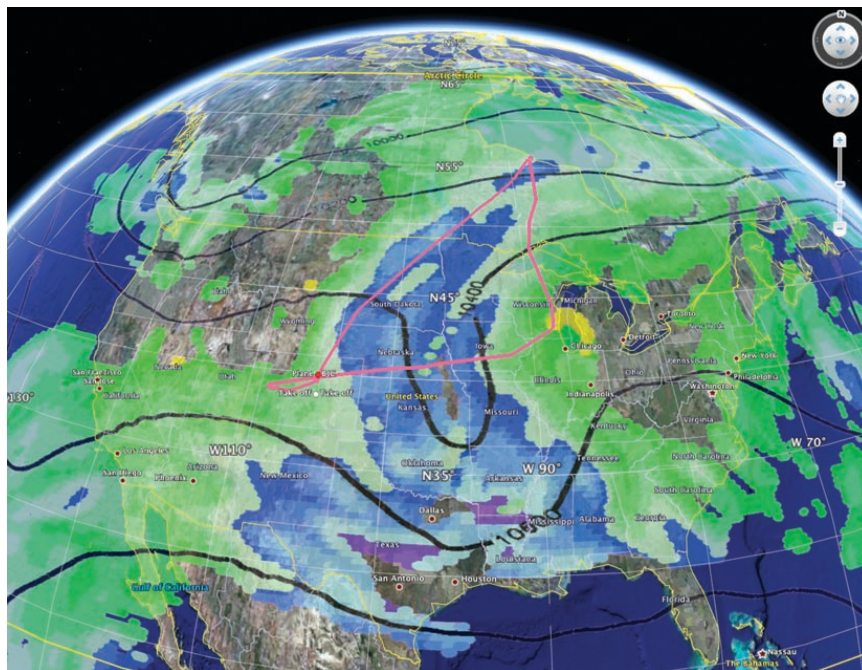


**FIG. 4.** Map shows areas with a double tropopause on 18 Apr 2008. All color-shaded regions are having a double tropopause based on the 1800 UTC GFS analysis. The color indicates the minimum static stability (in terms of potential temperature lapse rate  $d\theta/dz$ , in  $\text{K km}^{-1}$ ) between the primary and secondary tropopauses. For a vertical cross section that explicitly shows the tropopause heights, see Fig. 5. The red line marks the ground track for RF01. The black contours are the geopotential height at 250 hPa.

**Stratospheric intrusion: RF04, 28 April 2008.** Following the pioneering work of Danielsen (1968), stratospheric intrusions, in the form of tropopause folds, have been the focus of a number of research aircraft investigations (e.g., Shapiro 1980; Browell et al. 1987; Cooper et al. 2004, 2005; Pan et al. 2007). The preferred region of these events has been examined on a global scale using PV analyses (Elbern et al. 1998; Sprenger et al. 2003). The current interest of such events largely relates to the impact on tropospheric ozone and the behavior of the tropopause during this type of active two-way exchange event. Since dynamical variables, such as PV, and chemical variables, such as ozone, may not have the same lifetime in the tropopause region, meteorological analyses alone are not able to quantify the impact of folding events on the chemical structure of the UTLS. The START08 mission was able to map the chemical structure of stratospheric intrusions using the large suite of tracer instruments on the GV. The ultimate goal is to link the dynamical and the chemical behavior of the process. In particular, we will examine the irreversible mixing during folding and its impact on chemical and dynamical variables. Some initial results from RF04 are given as examples.

Flight RF04 targeted a stratospheric intrusion event on 28 April 2008 associated with a long narrow trough over the central United States. The northerly polar jet accompanying this sharp trough (Fig. 7) merged with the subtropical jet over Mississippi and Alabama. In Fig. 8 the fold can be seen as the 2-PVU ( $1 \text{ PVU} = 10^{-6} \text{ m}^2 \text{ K kg}^{-1} \text{ s}^{-1}$ ) potential vorticity surface (purple) intruding underneath the jet (blue). The flight strategy not only targets the airmass contrast inside and outside the fold, as did in earlier studies (Danielsen 1968; Shapiro 1980), but also the vertical chemical discontinuity at the tropopause in the vicinity of the fold. The aircraft made several transects across the jet and the fold at different altitudes along approximately 40°N. Several complete profiles from ~3 to ~14 km were flown to map out the chemical gradient on both cyclonic and anticyclonic sides of the jet. In the region of the fold, the thermal tropopause (yellow) is widely separated from the 2-PVU surface, reflecting a weak thermal gradient in the region. The correlation between ozone and CO further indicates that a broad layer of mixed stratospheric and tropospheric air exists in the region of the fold. The stratospheric intrusion is therefore responsible for a deep extratropical transition layer (ExTL;

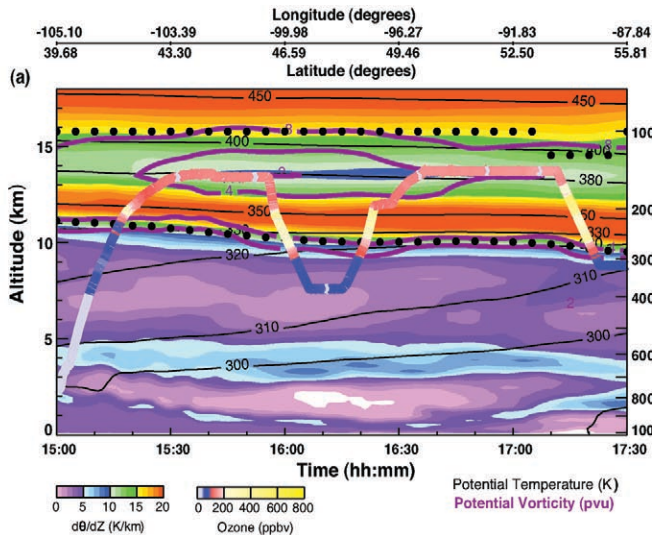


FIG. 5. (a) Vertical section of selected dynamical variables along the first leg of the RF01 flight track (Colorado to Hudson Bay; see Fig. 4). Colored image indicates the static stability in terms of the potential temperature lapse rate as in Fig. 4. The typical tropospheric condition is represented by purple shades (up to  $5 \text{ K km}^{-1}$ ). The typical stratospheric condition is represented by the yellow–red shades ( $>15 \text{ K km}^{-1}$ ). The blue and green shades indicate transitional conditions ( $5\text{--}15 \text{ K km}^{-1}$ ). Potential vorticity contours are shown in purple, and the tropopause height (including both the primary and the secondary tropopause) based on GFS is represented by black dots. The GV flight track (multicolored line) is colored according to the in situ ozone values. (b) Selected measurements for the same leg. The aircraft flight level (gray), flight-level potential temperature (blue), ozone (red), and carbon monoxide (green) are shown.

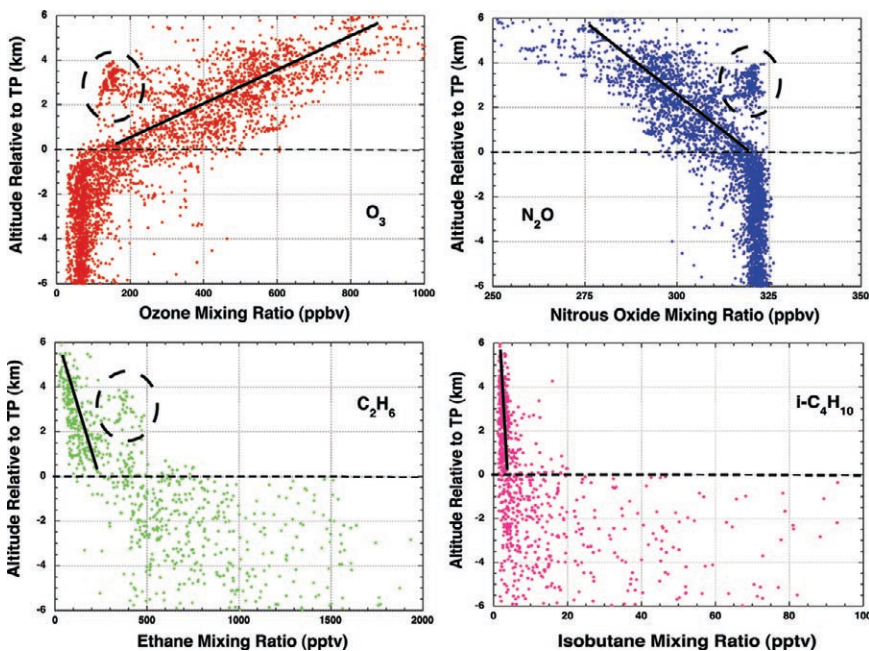
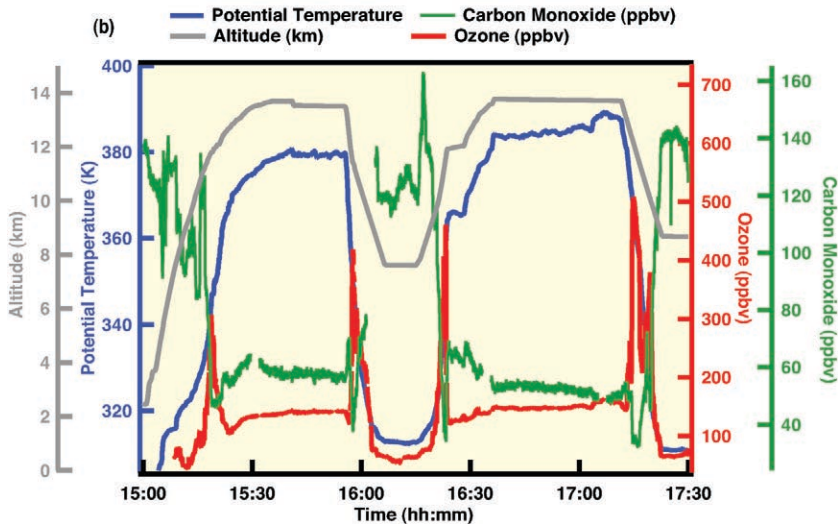
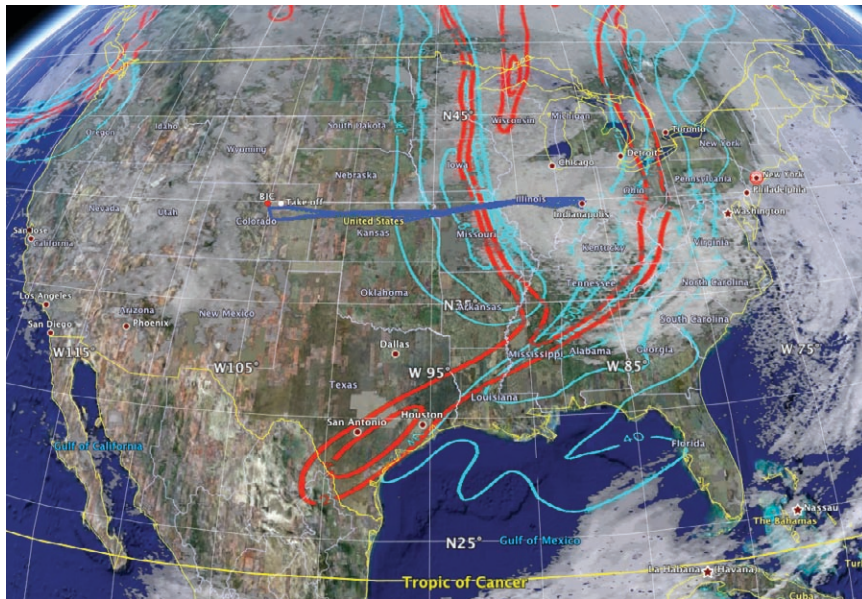


FIG. 6. Values of ozone ( $\text{O}_3$ ), nitrous oxide ( $\text{N}_2\text{O}$ ), ethane ( $\text{C}_2\text{H}_6$ ), and isobutane ( $i\text{-C}_4\text{H}_{10}$ ) from all flights during START08 as a function of altitude relative to the tropopause. The ozone data are from the NOAA UV ozone photometer, subsampled at a 10-s rate. The nitrous oxide data are from the UCATS instrument. Ethane and isobutane are from the AWAS instrument. The black lines indicate the expected stratospheric behavior for these species. The dashed circles mark the anomalous concentration due to the influence of the tropospheric intrusions.



**FIG. 7 (TOP).** Synoptic-scale meteorological background for 28 Apr 2008 and the ground track of RF04 (dark blue). Jet streams are indicated by 300-hPa isotachs (light blue). UTLS boundary and horizontal gradients at this level are shown by 2- and 4-PVU contours (red).

**FIG. 8 (BOTTOM).** Stratospheric intrusion sampled during RF04, 28 Apr 2008. (top) The 3D structure of the thermal (yellow) and dynamical tropopause (2-PVU surface, purple), based on 1800 UTC GFS analyses, and the GV flight track (black line). (bottom) The 2D cross section approximately along 40°N latitude. Selected meteorological fields based on GFS analyses are shown [the thermal tropopause (cyan), potential temperature (magenta), PV including the 2-PVU contour (black), and the jet core position (gray shaded)]. The GV track is colored according to an O<sub>3</sub>-CO correlation-based airmass identification (Pan et al. 2004) indicating stratospheric (red), tropospheric (green), and mixed (blue).

WMO 2003), a region strongly influenced by mixing. Further analyses will examine the impact of the event to all trace gas species measured; the relation-

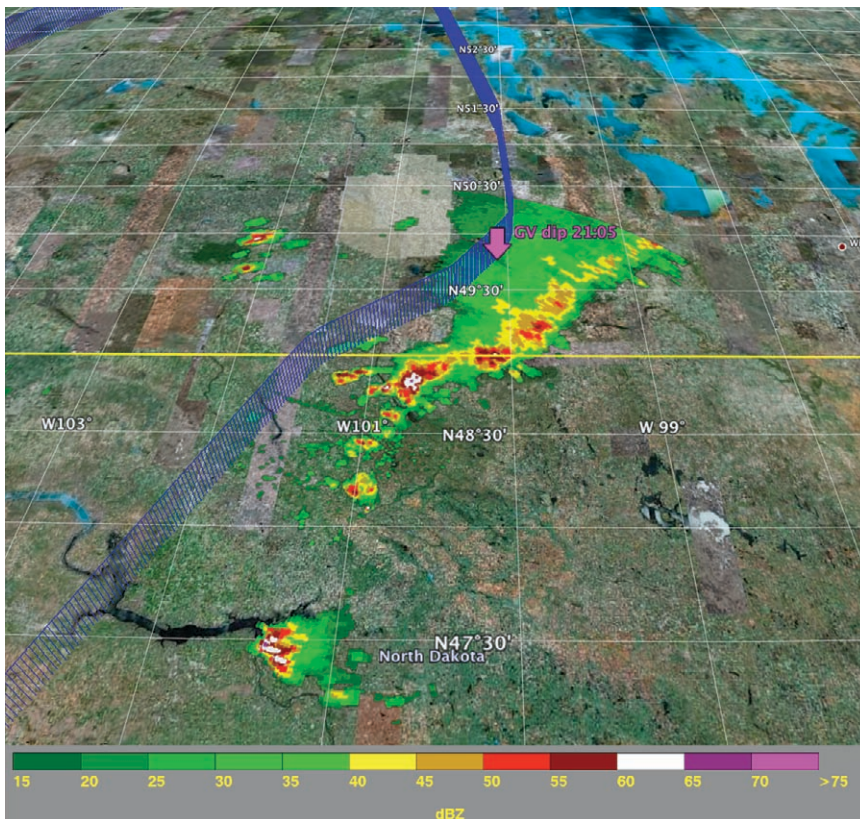
ship of chemical species and dynamical variables such as PV; the origins and the fate of the air mass involved; and how well these events are represented in models.

*Convective influence: RF14, 18 June 2008.* Thunderstorms alter the chemical composition of the UT and sometimes the LS through rapid vertical transport of insoluble constituents from near the boundary layer and through the production of NO during lightning discharges. The extent and variety of constituents added to the UT will depend on the proximity of the thunderstorm to boundary layer pollution or to locations of strong ecosystem emissions and on the frequency and strength of lightning activity. Additions of NO from lightning and aircraft or vertical transport of other precursors to peroxy radical formation are a significant source of ozone production in the UT on regional and global scales (e.g., Pickering et al. 1998; Cooper et al. 2007; Hudman et al. 2007).

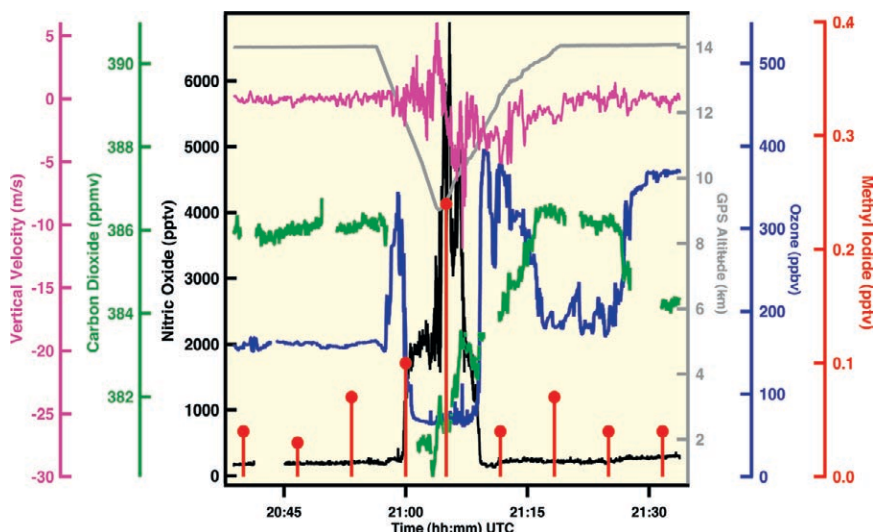
In situ study of the hostile environment of thunderstorms using instrumented aircraft is a challenge (Ridley et al. 2004a; Schumann and Huntrieser 2007). Forecasting storm development often has considerable uncertainty in space and time, making flight planning difficult. Portions of several flights were used as a learning experience for future investigations of deep convection using the GV.

**FIG. 9 (TOP).** Portion of the GV flight track during RF14, 18 Jun 2008, and radar reflectivity from Minot, ND, at 2056 UTC. The yellow line is the U.S.–Canada border. In situ measurements during a GV dip centered at 2105 UTC are shown in next figure.

**FIG. 10 (BOTTOM).** In situ measurements during RF14 on 18 Jun 2008 in the vicinity of the MCS shown in Fig. 9, including GV altitude (gray), flight-level vertical motion (magenta), and several chemical tracers such as nitric oxide (black) from the NCAR NO/NO<sub>y</sub> instrument, ozone (blue) from the NCAR fast-ozone instrument, carbon dioxide (green) from the Harvard/HAIS QCLS, and methyl iodide (red) from the HAIS/AWAS.



As an example, RF14 allowed limited sampling of a highly electrically active mesoscale convective system (MCS) that extended over North Dakota and southern Manitoba, Canada. Figure 9 shows the ground track of the GV superimposed on a radar reflectivity image of cloud field and radar reflectivity. The top of the convection was near 220 hPa. Figure 10 shows that the GV descended from 14 km into the storm clouds to just below 9 km where conditions became sufficiently turbulent, as indicated by the vertical wind variations from  $\sim +6$  to  $-10$  m s<sup>-1</sup>,



that the GV ascended to its original altitude above the MCS. The figure also shows that enhancements in NO up to 4–7 ppbv were observed between 9 and 10 km, indicative of the lightning activity. These mixing ratio enhancements are comparable to observations of lightning production of NO made in thunderstorm studies over the U.S. Midwest (Dye et al. 2000) but not as large as observed in some storms over Florida (Ridley et al. 2004b). In situ tracers also provided

signatures of convective transport. In the center of the convectively influenced air, low CO<sub>2</sub> concentration is indicative of biogenic uptake in the boundary layer and subsequent rapid vertical transport. Similarly, many short-lived species with emissions in the boundary layer and normally low mixing ratios in the UT were found to be significantly enhanced within the convective updraft. As an example, methyl iodide (lifetime  $\sim 4$  days) is shown here. Finally, ozone variations reflect the complex flow around the convective

system that influence UT composition. Higher ozone at the boundary of the convective cloud suggests entrainment of air from the lower stratosphere, whereas the central convective updraft contains low ozone, typical of the boundary layer input. Further analyses of this and other cases of storm-influenced air will focus on characterizing convective transport signature and time scale using the tracers and the lightning impact of NO in the upper troposphere.

**Gravity wave: RF02, 21 April 2008.** Gravity waves are known to play an important role in the UTLS. In situ measurement of terrain-induced GWs in the extratropical UTLS region was a focus of a previous campaign with the GV aircraft (Grubišić et al. 2008), but the role of jets and fronts in GW generation is not well understood (Zhang 2004). Systematic observations of jets and fronts as GW sources do not exist. One goal of START08 is to test how well the current generation of mesoscale models predicts the excitation of GWs by jets and fronts (Wu and Zhang 2004) and how tracer measurements can contribute to our understanding of GW breaking in the UTLS (Koch et al. 2005).

Flight RF02 on 21 April 2008 focused on GW excitation from both jet/front and topography. The flight tracks followed regions where gravity wave generation was predicted by the real-time mesoscale analysis and forecast system using the Advanced Research WRF model (Skamarock et al. 2005) and an ensemble-based multiphysics data assimilation (Meng and Zhang et al.

2008a,b; Fig. 11). The GV ground track indicates the sampling path in relation to the wave structure for an 8-h flight mostly in the lower stratosphere at an altitude between 10 and 13 km. The GV measurements of flight-level vertical motions show significant GW with wavelengths ranging from 10 to 300 km. These wave signatures are present in almost every leg of the 8-h flight, mostly in the lower stratosphere. Figure 12 displays a 2-h segment of the flight (from point B to point A). Initial analysis shows that the mesoscale component of the GW measured during the flight had qualitative agreement to those predicted by the 15-km mesoscale model forecast. This result represents the first successful mesoscale model prediction and high-resolution in situ measurement of these types of gravity waves by a research aircraft. Future work will examine the origin, dynamics, and impacts of these gravity waves.

**Profiling CO<sub>2</sub> from boundary layer to stratosphere.** The objectives of the pre-HIPPO flights were to test flight patterns, instruments, and support requirements for upcoming pole-to-pole global operations. During the START08 experiment, in addition to the payload verification, a strategy of routine sampling from the surface to ~14 km was successfully tested. A typical pre-HIPPO flight pattern, shown in Fig. 13, consists of multiple deep profiles. Profiling into the boundary layer, as low as ~100 m above the surface, was typically accomplished by executing preplanned missed

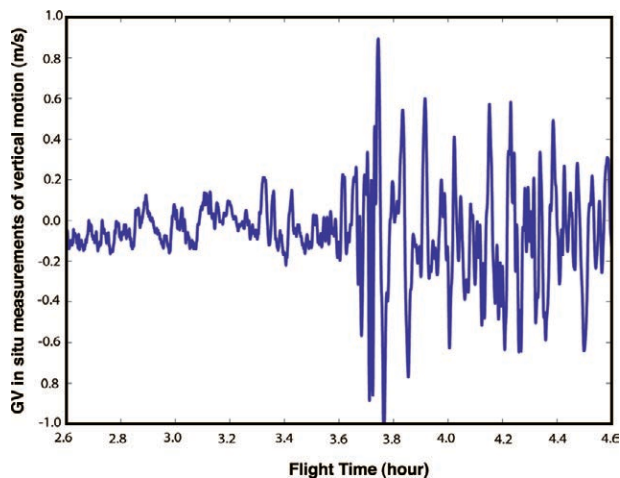
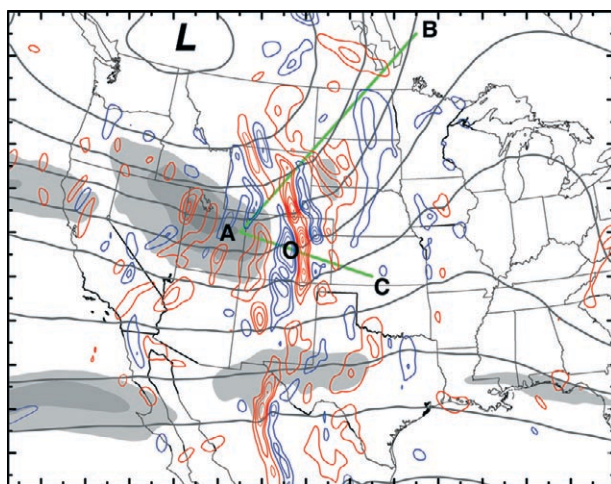


**FIG. 11 (LEFT).** The real-time mesoscale forecast of gravity waves valid at 2100 UTC 21 Apr for RF02. Plotted are the 12-km pressure (gray contours, every 3 hPa), vertical velocity (every 3 cm s<sup>-1</sup>; positive, blue; negative, red), and horizontal wind speed (shaded every 5 m s<sup>-1</sup> for values >40 m s<sup>-1</sup>). The green lines are the approximate flight tracks with A, B, and C as the flight turning points and point O as the location of the Rocky Mountain Metro Airport.

**FIG. 12 (RIGHT).** The GV flight-level aircraft measurement of vertical velocity (m s<sup>-1</sup>) during a 2-h segment of RF02 when the aircraft was flying from point B to point A, denoted in Fig. 11. A 60-s running average is applied to the raw aircraft data. The average air speed for this leg was ~220 m s<sup>-1</sup>.

approaches at selected airports. In addition to payload and flight operation development, pre-HIPPO flights sampled the dramatic seasonal change of CO<sub>2</sub> flux (Fig. 14). Cross sections of CO<sub>2</sub> and other trace gases were sampled from ~25°N (Gulf of Mexico) to ~65°N (Hudson Bay and Yellowknife, Canada) for both the spring and the summer seasons.

### SUMMARY AND OUTLOOK.

The START08 experiment succeeded in measuring chemical distributions, variations, and relationships associated with major transport processes in the UTLS region and in observing the different chemical gradient across “flat” and “structured” tropopause regions. Deep intrusions of tropospheric air into the lowermost stratosphere associated with the secondary tropopause were observed in situ for the first time with an extensive chemistry payload. The data analyses and modeling of the observed events should bring new insight into the mechanisms that control the chemical composition of the UTLS. Chemical tracers with different emission regions and with a wide range of lifetimes were sampled under a wide range of meteorological conditions. These measurements establish the START08 dataset as a significant asset for quantifying time scales of the relevant transport processes and for connecting meteorological fields to the chemical composition. The suite of tracers also presents a unique opportunity to characterize the chemical age and age spectra (e.g., Schoeberl et al. 2005) of the UTLS region under different conditions. Age spectra and age-of-air characterizations have been useful diagnostics for evaluating stratospheric transport in large-scale models (Waugh and Hall 2002 and references therein). The measurements from START08 provide the opportunity to extend these diagnostics to shorter time scales and especially for the UTLS, a region of active stratosphere–troposphere interactions (e.g., Ehhalt et al. 2007; Scheeren et al. 2003).



FIG. 13. GV flight track for RF10 from Colorado to Hudson Bay showing the “missed approach” flight pattern and the GFS tropopause (as in Fig. 8) for 1800 UTC 12 May 2008.

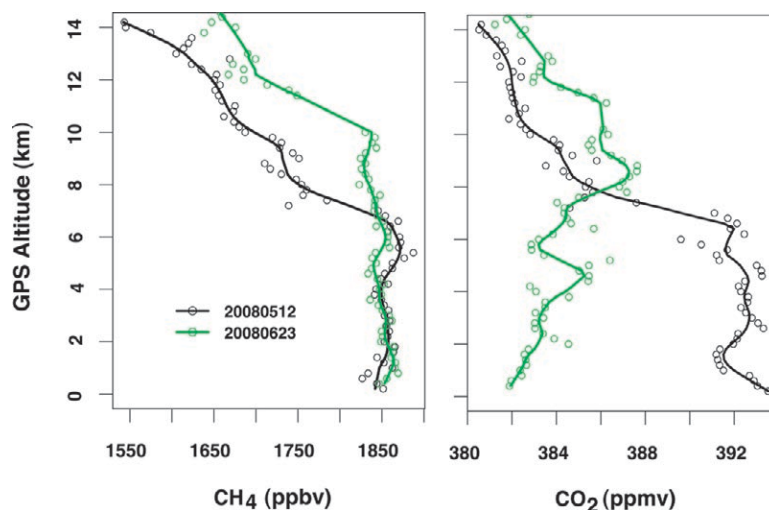


FIG. 14. Vertical profiles of methane (CH<sub>4</sub>) and carbon dioxide (CO<sub>2</sub>) over the Hudson Bay lowlands on 12 May (RF10) and 23 Jun (RF15) 2008. The profiles show seasonal deepening of the troposphere (shown in CH<sub>4</sub> profiles) and the change in the near-surface gradient of CO<sub>2</sub>, reflecting emissions of CO<sub>2</sub> by the land biosphere in May and uptake in Jun. The data points represent a binned average over a 200-m vertical range. The lines are produced by a fit with a low-pass filter.

Detailed comparisons of models and observations, along with process studies, will be major components of the postcampaign analyses. A planned intercomparison of model simulations from WACCM and CLaMS, one in an Eulerian and one in a Lagrangian framework, will examine the strengths and weaknesses of each framework in representing the tracer structure in the tropopause region and the mixing processes that occur under different dynamical con-

ditions. Moreover, high-resolution cloud-resolving simulations with the Advanced Research WRF model will be used to explore the dynamics and impacts of smaller-scale processes such as gravity waves, convection, and turbulence in the UTLS region.

With the extensive spatial coverage and variety of dynamical conditions sampled, START08 data make an important addition to an aircraft-based UTLS trace gas climatology (Tilmes et al. 2010, manuscript submitted to *J. Geophys. Res.*). The statistical characteristics of UTLS chemical constituents will be an important reference for CCMs and for validating satellite data. These are among a wide range of problems START08 team and collaborators will pursue as part of the postcampaign research activities.

**ACKNOWLEDGMENTS.** The START08 experiment is sponsored by the National Science Foundation (NSF). A large number of people contributed to the success of the START08 experiment. The dedication of the instrument team, co-sponsored by NCAR, the University of Colorado, Harvard University, the University of Miami, Princeton University, the NOAA/Earth System Research Laboratory (ESRL) Global Monitoring Division (GMD) and Chemical Science Division (CSD), and the NCAR Research Aviation Facility staff in running the flight operation was the key factor in the success of campaign. We also acknowledge the efforts and skills of the GV pilots Henry Boynton and Ed Ringleman, which were critical to meeting mission objectives. We thank colleagues from NCEP Environmental Modeling Center for providing special high-resolution output of GFS data. The mesoscale model forecast and post analyses are sponsored by NSF Grants ATM-0618662 and ATM-0904635 and co-sponsored by Texas A&M University and the Pennsylvania State University. Additional forecast effort is supported by NSF Grant ATM-0722225 to Texas A&M University.

## REFERENCES

- Bowman, K. P., L. L. Pan, T. Campos, and R. Gao, 2007: Observations of fine-scale transport structure in the upper troposphere from the High-Performance Instrumented Airborne Platform for Environmental Research. *J. Geophys. Res.*, **112**, D18111, doi:10.1029/2007JD008685.
- Browell, E., E. Danielsen, S. Ismail, G. Gregory, and S. Beck, 1987: Tropopause fold structure determined from airborne lidar and in situ measurements. *J. Geophys. Res.*, **92** (D2), 2112–2120.
- Cooper, O., and Coauthors, 2004: On the life cycle of a stratospheric intrusion and its dispersion into polluted warm conveyor belts. *J. Geophys. Res.*, **109**, D23S09, doi:10.1029/2003JD004006.
- , and Coauthors, 2005: Direct transport of mid-latitude stratospheric ozone into the lower troposphere and marine boundary layer of the tropical Pacific Ocean. *J. Geophys. Res.*, **110**, D23310, doi:10.1029/2005JD005783.
- , and Coauthors, 2007: Evidence for a recurring eastern North America upper tropospheric ozone maximum during summer. *J. Geophys. Res.*, **112**, D23304, doi:10.1029/2007JD008710.
- Danielsen, E. F., 1968: Stratospheric–tropospheric exchange based on radioactivity, ozone, and potential vorticity. *J. Atmos. Sci.*, **25**, 502–518.
- Dobson, G. M. B., 1973: The laminated structure of the ozone in the atmosphere. *Quart. J. Roy. Meteor. Soc.*, **99**, 599–607.
- Dye, J. E., and Coauthors, 2000: An overview of the STERAO–Deep Convection Experiment with results for the 10 July storm. *J. Geophys. Res.*, **105**, 10 023–10 045.
- Ehhalt, D. H., F. Rohrer, D. R. Blake, D. E. Kinnison, and P. Konopka, 2007: On the use of nonmethane hydrocarbons for the determination of age spectra in the lower stratosphere. *J. Geophys. Res.*, **112**, D12208, doi:10.1029/2006JD007686.
- Elbern, H., J. Hendricks, and A. Ebel, 1998: A climatology of tropopause folds by global analyses. *Theor. Appl. Climatol.*, **59**, 181–200.
- Eyring, V., and Coauthors, 2005: A strategy for process-oriented validation of coupled chemistry–climate models. *Bull. Amer. Meteor. Soc.*, **86**, 1117–1133.
- Fischer, H., and Coauthors, 2000: Tracer correlations in the northern high-latitude lowermost stratosphere: Influence of cross-tropopause mass exchange. *Geophys. Res. Lett.*, **27**, 97–100.
- Forster, P. M., and K. P. Shine, 1997: Radiative forcing and temperature trends from stratospheric ozone changes. *J. Geophys. Res.*, **102** (D9), 10 841–10 855.
- Garcia, R. R., D. R. Marsh, D. E. Kinnison, B. A. Boville, and F. Sassi, 2007: Simulation of secular trends in the middle atmosphere, 1950–2003. *J. Geophys. Res.*, **112**, D09301, doi:10.1029/2006JD007485.
- Grubišić, V., and Coauthors, 2008: The Terrain-Induced Rotor Experiment. *Bull. Amer. Meteor. Soc.*, **89**, 1513–1533.
- Hints, E. J., and Coauthors, 1998: Troposphere-to-stratosphere transport in the lowermost stratosphere from measurements of H<sub>2</sub>O, CO<sub>2</sub>, N<sub>2</sub>O, and O<sub>3</sub>. *Geophys. Res. Lett.*, **25**, 2655–2658.
- Holton, J. R., P. H. Haynes, M. E. McIntyre, A. R. Douglass, R. B. Rood, and L. Pfister, 1995: Stratosphere–troposphere exchange. *Rev. Geophys.*, **33**, 403–439.

- Hoor, P., H. Fischer, L. Lange, J. Lelieveld, and D. Brunner, 2002: Seasonal variations of a mixing layer in the lowermost stratosphere as identified by the CO–O<sub>3</sub> correlation from in situ measurements. *J. Geophys. Res.*, **107**, 4044, doi:10.1029/2000JD000289.
- , C. Gurk, D. Brunner, M. I. Hegglin, H. Wernli, and H. Fischer, 2004: Seasonality and extent of extratropical TST derived from in situ CO measurements during SPURT. *Atmos. Chem. Phys.*, **4**, 1427–1442.
- Hudman, R. C., and Coauthors, 2007: Surface and lightning sources of nitrogen oxides over the United States: Magnitudes, chemical evolution, and outflow. *J. Geophys. Res.*, **112**, D12S05, doi:10.1029/2006JD007912.
- Kinnison, D. E., and Coauthors, 2007: Sensitivity of chemical tracers to meteorological parameters in the MOZART-3 chemical transport model. *J. Geophys. Res.*, **112**, D20302, doi:10.1029/2006JD007879.
- Koch, S. E., and Coauthors, 2005: Turbulence and gravity waves within an upper-level front. *J. Atmos. Sci.*, **62**, 3885–3908.
- Konopka, P., and Coauthors, 2007: Contribution of mixing to the upward transport across the TTL. *Atmos. Chem. Phys.*, **7**, 3285–3308.
- Marcy, T., and Coauthors, 2004: Quantifying stratospheric ozone in the upper troposphere with in situ measurements of HCl. *Science*, **304**, 261–265.
- McKenna, D. S., P. Konopka, J.-U. Grooß, G. Günther, R. Müller, R. Spang, D. Offermann, and Y. Orsolini, 2002: A new Chemical Lagrangian Model of the Stratosphere (CLaMS) 1. Formulation of advection and mixing. *J. Geophys. Res.*, **107** (D16), 4309, doi:10.1029/2000JD000114.
- Meng, Z., and F. Zhang, 2008a: Test of an ensemble Kalman filter for mesoscale and regional-scale data assimilation. Part III: Comparison with 3DVAR in a real-data case study. *Mon. Wea. Rev.*, **136**, 522–540.
- , and —, 2008b: Test of an ensemble Kalman filter for mesoscale and regional-scale data assimilation. Part IV: Comparison with 3DVAR in a month-long experiment. *Mon. Wea. Rev.*, **136**, 3671–3682.
- Pan, L. L., W. J. Randel, B. L. Gary, M. J. Mahoney, and E. J. Hints, 2004: Definitions and sharpness of the extratropical tropopause: A trace gas perspective. *J. Geophys. Res.*, **109**, D23103, doi:10.1029/2004JD004982.
- , and Coauthors, 2007: Chemical behavior of the tropopause observed during the Stratosphere–Troposphere Analyses of Regional Transport experiment. *J. Geophys. Res.*, **112**, D18110, doi:10.1029/2007JD008645.
- , and Coauthors, 2009: Tropospheric intrusions associated with the secondary tropopause. *J. Geophys. Res.*, **114**, D10302, doi:10.1029/2008JD011374.
- Pickering, K. E., Y. Wang, W.-K. Tao, C. Price, and J.-F. Müller, 1998: Vertical distributions of lightning NO<sub>x</sub> for use in regional and global chemical transport models. *J. Geophys. Res.*, **103**, 31 203–31 216.
- Randel, W. J., D. J. Seidel, and L. L. Pan, 2007: Observational characteristics of double tropopauses. *J. Geophys. Res.*, **112**, D07309, doi:10.1029/2006JD007904.
- Reed, R. J., 1955: A study of a characteristic type of upper-level frontogenesis. *J. Meteor.*, **12**, 226–237.
- Ridley, B., and Coauthors, 2004a: Convective transport of reactive constituents to the tropical and mid-latitude tropopause region: I. Observations. *Atmos. Environ.*, **38**, 1259–1274.
- , and Coauthors, 2004b: Florida thunderstorms: A faucet of reactive nitrogen to the upper troposphere. *J. Geophys. Res.*, **109**, D17305, doi:10.1029/2004JD004769.
- Scheeren, H. A., and Coauthors, 2003: Reactive organic species in the northern extratropical lowermost stratosphere: Seasonal variability and implications for OH. *J. Geophys. Res.*, **108**, 4805, doi:10.1029/2003JD003650.
- Schmidt, T., G. Beyerle, S. Heise, J. Wickert, and M. Rothacher, 2006: A climatology of multiple tropopauses derived from GPS radio occultations with CHAMP and SAC-C. *Geophys. Res. Lett.*, **33**, L04808, doi:10.1029/2005GL024600.
- Schoeberl, M. R., A. R. Douglass, B. Polansky, C. Boone, K. A. Walker, and P. Bernath, 2005: Estimation of stratospheric age spectrum from chemical tracers. *J. Geophys. Res.*, **110**, D21303, doi:10.1029/2005JD006125.
- Schumann, U., and H. Huntrieser, 2007: The global lightning-induced nitrogen oxides source. *Atmos. Chem. Phys.*, **7**, 3823–3907.
- Shapiro, M. A., 1980: Turbulent mixing within tropopause folds as a mechanism for the exchange of chemical constituents between the stratosphere and troposphere. *J. Atmos. Sci.*, **37**, 994–1004.
- Shepherd, T. G., 2007: Transport in the middle atmosphere. *J. Meteor. Soc. Japan*, **85B**, 165–191.
- Skamarock, W. C., J. B. Klemp, J. Dudhia, D. O. Gill, D. M. Barker, W. Wang, and J. G. Powers, 2005: A description of the Advanced Research WRF version 2. NCAR Tech. Note NCAR/TN-468+STR, 88 pp.
- Sprenger, M., and H. Wernli, 2003: A Northern Hemispheric climatology of cross-tropopause exchange for the ERA-15 time period (1979–1993). *J. Geophys. Res.*, **108**, 8521, doi:10.1029/2002JD002636.

- , M. Croci Maspoli, and H. Wernli, 2003: Tropopause folds and cross-tropopause exchange: A global investigation based upon ECMWF analyses for the time period March 2000 to February 2001. *J. Geophys. Res.*, **108**, 8518, doi:10.1029/2002JD002587.
- Stohl, A., Wernli, P. James, M. Bourqui, C. Forster, M. A. Liniger, P. Seibert, and M. Sprenger, 2003: A new perspective of stratosphere–troposphere exchange. *Bull. Amer. Meteor. Soc.*, **84**, 1565–1573.
- Vaughan, G., and C. Timmis, 1998: Transport of near-tropopause air into the lower midlatitude stratosphere. *Quart. J. Roy. Meteor. Soc.*, **124**, 1559–1578.
- Wang, S., and F. Zhang, 2007: Sensitivity of mesoscale gravity waves to the baroclinicity of jet-front systems. *Mon. Wea. Rev.*, **135**, 670–688.
- Waugh, D. W., and T. M. Hall, 2002: Age of stratospheric air: Theory, observations, and models. *Rev. Geophys.*, **40**, 1010, doi:10.1029/2000RG000101.
- Wernli, H., and M. Sprenger, 2007: Identification and ERA-15 climatology of potential vorticity streamers and cutoffs near the extratropical tropopause. *J. Atmos. Sci.*, **64**, 1569–1586.
- WMO, 2003: Scientific assessment of ozone depletion 2002. WMO Global Ozone Research and Monitoring Project Rep. 47, 498 pp.
- Wu, D. L., and F. Zhang, 2004: A study of mesoscale gravity waves over the North Atlantic with satellite observations and a mesoscale model. *J. Geophys. Res.*, **109**, D22104, doi:10.1029/2004JD005090.
- Young, L.-H., and Coauthors, 2007: Enhanced new particle formation observed in the northern midlatitude tropopause region. *J. Geophys. Res.*, **112**, D10218, doi:10.1029/2006JD008109.
- Zahn, A., and Coauthors, 2000: Identification of extratropical two-way troposphere–stratosphere mixing based on CARIBIC measurements of O<sub>3</sub>, CO, and ultrafine particles. *J. Geophys. Res.*, **105**, 1527–1535.
- Zhang, F., 2004: Generation of mesoscale gravity waves in the upper-tropospheric jet-front systems. *J. Atmos. Sci.*, **61**, 440–457.